

# Acute Radiation Risks Tool (ARRT) Development for the Upcoming Human Exploration Missions

Shaowen Hu<sup>1</sup>, Shayan Monadjemi<sup>2</sup>, Janet Elliott Barzilla<sup>3</sup>, and Edward Semones<sup>4</sup>

<sup>1</sup>KBR

<sup>2</sup>Washington University in St. Louis

<sup>3</sup>Unknown

<sup>4</sup>NASA Johnson Space Center

November 22, 2022

## Abstract

The health risks of space radiation present big challenges to space exploration, with the possibility of large Energetic Solar Particle Events (ESPEs) inducing Acute Radiation Sickness (ARS) during upcoming Artemis missions. An operational software Acute Radiation Risk Tool (ARRT) was developed to directly use measurements from onboard dosimeters to project organ doses during times of increased radiation exposure, so that any possible ARS risks of the astronauts can be modelled and monitored in real time using a data stream at the astronaut location. To enable ARRT to handle variant scenarios of any possible ESPEs in an automatic manner for mission operation, two datasets were employed in developing its modules, one involving historical solar protons recorded over the past four decades, and the other using the real-time telemetry readings of dosimeters onboard International Space Station (ISS). Though vastly different in term of data cadence, smoothness, and data gaps, all events in these datasets can be correctly processed to output organ doses and ARS risks and generate flight notes for communication within the Flight Control Team (FCT). All these tasks are completed with close interactions between multiple modules developed with many state-of-the-art facilities of full stack web applications. This work demonstrates that ARRT meets the requirement to project radiation exposure and to provide clinical guidelines in very short time steps as the ESPE unfolds, even for the longest event in datasets, making this tool eligible to be tested during the upcoming unmanned Artemis mission and utilized in future space exploration.



*Space Weather*

Supporting Information for

**Acute Radiation Risks Tool (ARRT) Development for the Upcoming Human Exploration Missions**

S. Hu <sup>1</sup>, S. Monadjemi <sup>2</sup>, J. E. Barzilla <sup>3</sup>, and E. Semones <sup>4</sup>

<sup>1</sup> KBR, Houston, TX, <sup>2</sup> Washington University in St. Louis, St. Louis, MO, <sup>3</sup> Leidos, Houston, TX, <sup>4</sup> NASA Johnson Space Center, Houston TX

## Categories of ARS impacts and recommendations for flight notes

The severity of various ARS symptoms can be calculated with biomathematical models developed for neurovascular system and hematopoietic system, which are highly dose dependent according to previous investigations (Hu et al., 2009; 2011; 2012; 2015). Therefore, they can be categorized solely from the total BFO doses as estimated from the organ dose projection algorithm and can be roughly scored similar to the Response Category system (Fliedner et al., 2001). The scores for NV (nausea/vomiting), FW (fatigue/weakness), and HG (HemoGrade) in the following categories are estimated by assuming acute exposure at different levels, while the textual descriptions are giving based on Tables 1 and 2, as well as SRAG space weather console practice. For protracted exposure like during typical ESPEs, the neurovascular effects may be less severe than predicted this way.

Because the current NASA short-term (30 days) permissible exposure limit (PEL) for acute radiation effects is 250 mGy-Eq to the blood forming organs (BFO) (NASA, 2014), focus of this categorization for near future deep space exploration should be those in the low dose range. As discussed in the introduction section, generally SPEs can be effectively shielded, and current vehicle designs incorporate smart shielding concepts such as the redistribution of vehicle mass in MPCV. In addition, an effective warning system for a large SPE could also help to reduce the event exposure. Therefore, it is unlikely that astronauts inside an interplanetary spacecraft will experience the full spectrum of following health impacts. Nevertheless, significant exposure on lunar or planetary surfaces is possible if the crew is not well protected, and the various acute risks depicted below should be of concerns.

Short term crew impacts:

1. 0-100 mGy-eq: (NV1-FW1-HG0) The accumulative dose will not induce any effects of acute radiation syndrome over the next 48 hours.
2. 100-250 mGy-eq: (NV1-FW1-HG0) Prodromal effects are not expected during the next two days; however, crew is encouraged to report symptoms of fatigue or nausea to Surgeon.
3. 250-500 mGy-eq: (NV1-FW1-HG1) Prodromal effects are not expected during the next two days; however, crew is encouraged to report symptoms of fatigue or nausea to Surgeon. Bloodwork may indicate an asymptomatic low-to-normal lymphocyte concentration.
4. 500-1000 mGy-eq: (NV2-FW2-HG2) Symptoms such as nausea and anorexia may appear within 24 hours of exposure, manifested as an upset stomach with clammy/sweaty skin and watering mouth. Complete disappearance of these symptoms is certain within 48 hours of exposure. Fatigue and mild weakness may appear during this time period. Bloodwork will indicate a mostly asymptomatic decrease in lymphocyte concentration.
5. 1000-1500 mGy-eq: (NV3-FW2-HG2) Within the first hours after exposure, crew may experience mild nausea and anorexia accompanied by considerable sweating and frequent swallowing to avoid vomiting. Symptoms are expected to persist for two days. Fatigue and mild weakness are possible. Bloodwork may indicate a rapid decrease in lymphocyte concentration.
6. 1500-2000 mGy-eq: (NV3-FW3-HG2) Within the first hours after exposure, crew may experience moderate nausea and anorexia accompanied by a few episodes of vomiting. Symptoms are expected to persist for two days. Fatigue and moderate weakness are possible. Bloodwork may indicate a rapid decrease in lymphocyte concentration.
7. 2000-3000 mGy-eq: (NV3-FW3-HG3) The crew will vomit several times, experiencing dry heaves and severe nausea. Fatigue and moderate weakness will appear. Bloodwork may indicate a rapid decrease in lymphocyte count.
8. > 3000 mGy-eq: (NV4-FW3-HG3) The crew will vomit several times, experiencing dry heaves and severe nausea. Fatigue and weakness will appear. Bloodwork may indicate a rapid decrease in lymphocyte count and increase in granulocyte count.

Continuing crew impacts:

1. 0-100 mGy-eq: (NV1-FW1-HG0) No symptoms of acute radiation syndrome are expected over the next

six weeks. The crew should make a best effort to keep the exposure as low as reasonably achievable, per the As Low As Reasonably Achievable (ALARA) principle to minimize potential late health impacts such as cancer, cataracts, heart disease, and damage to the central nervous system.

2. 100-250 mGy-eq: (NV1-FW1-HG0) No acute radiation syndrome symptoms are expected during the next six weeks. Bloodwork may indicate an asymptomatic low-to-normal concentration of lymphocytes, platelets and granulocytes. The crew should make a best effort to keep the exposure as low as reasonably achievable (i.e., the ALARA principle) to minimize potential late health impacts such as cancer, cataracts, heart disease, and damage to central nervous system.
3. 250-500 mGy-eq: (NV1-FW1-HG1) No acute radiation syndrome symptoms are expected during the next six weeks. Bloodwork may indicate an asymptomatic decrease in the concentration of lymphocytes, platelets, and granulocytes to the lower end of the normal range. The crew should make a best effort to keep the exposure as low as reasonably achievable (i.e., the ALARA principle) to minimize potential late health impacts such as cancer, cataracts, heart disease, and damage to central nervous system.
4. 500-1000 mGy-eq: (NV2-FW2-HG2) Fatigue and weakness may persist for several weeks. The crew are at low risk of developing infectious diseases or bleeding due to a decrease in concentrations of lymphocytes, platelets, and granulocytes below the lower end of the normal range. Autologous recovery is certain.
5. 1000-1500 mGy-eq: (NV3-FW2-HG2) Fatigue and weakness may persist for several weeks. The crew are at risk of developing infectious diseases or bleeding due to a decrease in concentrations of lymphocytes, platelets, and granulocytes below the lower end of the normal range. Autologous recovery is certain.
6. 1500-2000 mGy-eq: (NV3-FW3-HG2) Fatigue and weakness may persist for several weeks. The crew are at a high risk of developing infectious diseases or bleeding due to a decrease in concentrations of lymphocytes, platelets, and granulocytes far below the lower end of the normal range. Autologous recovery is certain.
7. 2000-3000 mGy-eq: (NV3-FW3-HG3) Severe nausea and vomiting may recur after two days, with fatigue and weakness persisting for several weeks. The crew are at a high risk of developing infectious diseases or bleeding due to a decrease in concentrations of lymphocytes, platelets, and granulocytes far below the lower end of the normal range. Autologous recovery is still certain.
8. > 3000 mGy-eq: (NV4-FW3-HG3) Severe nausea and vomiting may recur after two days, with fatigue and weakness persisting for several weeks. The crew are at a very high risk of developing infectious diseases or bleeding due to a decrease in concentrations of lymphocytes, platelets, and granulocytes far below the lower end of the normal range. Autologous recovery is possible.

1 **Acute Radiation Risks Tool (ARRT) Development for the Upcoming Human**  
2 **Exploration Missions**

3  
4 **S. Hu<sup>1</sup>, S. Monadjemi<sup>2</sup>, J. E. Barzilla<sup>3</sup>, and E. Semones<sup>4</sup>**

5  
6 <sup>1</sup>KBR, Houston, TX.

7 <sup>2</sup>Washington University in St. Louis, St. Louis, MO.

8 <sup>3</sup>Leidos, Houston, TX.

9 <sup>4</sup>NASA Johnson Space Center, Houston TX.

10  
11 Corresponding author: Shaowen Hu ([shaowen.hu-1@nasa.gov](mailto:shaowen.hu-1@nasa.gov))

12 **Key Points:**

- 13
- 14 • An algorithm to use onboard dosimeter readings to assess acute risks for future space exploration missions is developed into a web tool
  - 15 • This tool represents a good example of effort to transition research to operations
  - 16 • Many state-of-the-art facilities of full stack web applications and advanced computational
  - 17 techniques are essential to the development
- 18  
19

20  
21  
22  
23  
24  
25  
26  
27  
28  
29  
30  
31  
32  
33  
34  
35  
36  
37  
38  
39  
40  
41

## **Abstract**

The health risks of space radiation present big challenges to space exploration, with the possibility of large Energetic Solar Particle Events (ESPEs) inducing Acute Radiation Sickness (ARS) during upcoming Artemis missions. An operational software Acute Radiation Risk Tool (ARRT) was developed to directly use measurements from onboard dosimeters to project organ doses during times of increased radiation exposure, so that any possible ARS risks of the astronauts can be modelled and monitored in real time using a data stream at the astronaut location. To enable ARRT to handle variant scenarios of any possible ESPEs in an automatic manner for mission operation, two datasets were employed in developing its modules, one involving historical solar protons recorded over the past four decades, and the other using the real-time telemetry readings of dosimeters onboard International Space Station (ISS). Though vastly different in term of data cadence, smoothness, and data gaps, all events in these datasets can be correctly processed to output organ doses and ARS risks and generate flight notes for communication within the Flight Control Team (FCT). All these tasks are completed with close interactions between multiple modules developed with many state-of-the-art facilities of full stack web applications. This work demonstrates that ARRT meets the requirement to project radiation exposure and to provide clinical guidelines in very short time steps as the ESPE unfolds, even for the longest event in datasets, making this tool eligible to be tested during the upcoming unmanned Artemis mission and utilized in future space exploration.

## **Plain Language Summary**

42  
43  
44  
45  
46  
47  
48  
49  
50  
51

An operational tool ARRT was developed to directly use the onboard dosimeters' reading as inputs to estimate organ dose and possible clinical acute effects in case of severe Solar Particle Events (SPEs) for the upcoming Artemis missions. This paper describes all underlying models of the tool, various functions essential to operational management of possible effects, and how they are integrated to run automatically in real time whether the dosimeter readings are at background range or are elevated. A historical dataset with recorded 159 significant events is used to demonstrate its flexibility and accuracy to process diverse features of SPEs.

## **1 Introduction**

52  
53  
54  
55  
56  
57  
58  
59  
60  
61  
62  
63  
64

Leaving the protection of the Earth's atmosphere and geomagnetic field, astronauts travelling in deep space are at risk from radiation hazards induced by various high energy particles ubiquitous in our solar system. In the literature, much of the focus has been on the high energies of Galactic Cosmic Rays (GCR), which are hard to shield and may induce stochastic late health effects such as cancers that are of post-flight concern. Additionally, the intense Energetic Solar Particle Events (ESPEs) can cause Acute Radiation Sickness (ARS) that could manifest during the mission. Previous analyses indicate that ARS symptoms would be generally mild to moderate even in the worst case SPEs for crew inside a typical interplanetary spacecraft (Townsend et al., 1991, 2018), but even mild manifestations of fatigue and nausea could make the impacted crew less able to perform required tasks and thus may adversely impact the success of a mission (Hu et al., 2009). As opposed to GCR, SPEs can be effectively shielded against, and recent vehicle designs have incorporated shielding concepts that make use of the redistribution of vehicle mass.

65 An effective warning system for a large SPE could also allow the crew additional time to  
66 reconfigure the vehicle volume and reduce their event exposure.

67  
68 As SPEs are not always directed to the measuring satellites deployed either close to the Earth or  
69 in interplanetary space, a practical way to estimate the ARS risks for future exploration  
70 spaceflights like Mars missions will be through the use of onboard dosimeters. Using direct  
71 measurements, radiation exposure can be monitored both in real-time and always along the path  
72 of the spacecraft. Such an algorithm has been developed specifically for the Orion Multi-Purpose  
73 Crew Vehicle (MPCV) and described in a recent publication (Mertens et al., 2018). This organ  
74 dose estimation algorithm involves a fitting procedure between the real-time vehicle dosimeter  
75 measurements and a precomputed database of dose quantities calculated from the HZETRN  
76 radiation transport code (Slaba et al., 2016; Wilson et al., 2016), considering the actual MPCV  
77 vehicle geometry and mass distribution. The paper also described how the estimated organ doses  
78 at the crew locations are utilized as inputs to a set of biological response models, which predict  
79 clinically critical syndromes associated with ARS and quantify Radiation-Induced Performance  
80 Decrement (RIPD) (Hu & Cucinotta, 2011; Hu et al., 2009, 2012). The modeled results will  
81 provide important information to guide the crew mitigation efforts in case of severe ESPEs  
82 through the efforts of FCT.

83 The organ dose fitting algorithm, as well as the biomathematical ARS models, have been  
84 incorporated in a software package, the Acute Radiation Risks Tool (ARRT), which is currently  
85 planned to test operationally on NASA's next unmanned beyond-Low Earth Orbit (LEO)  
86 mission (Artemis I at the time of this writing) and will be fully utilized on the following manned  
87 beyond-LEO mission (Artemis II at the time of this writing) (Hu et al., 2020). During a space  
88 flight mission, ARRT will be run at the Mission Control Center (MCC), and all its outputs will  
89 be automatically produced at the telemetry time cadence of the vehicle dosimeter measurements,  
90 which is anticipated in the range of 15 to 30 minutes. The operationally useful functions of the  
91 tool include rendering and plotting the dosimeter readings, detecting the onset and end of an  
92 event, calculating and plotting the relevant organ dose quantities, triggering the ARS biological  
93 models if threshold is reached, and generating a flight note to facilitate communication of a  
94 mitigation response within FCT. This paper attempts to give a summary of these functions and to  
95 describe how they are developed in a compact software tool. Section 2 briefly describes the  
96 algorithms underlying various models, Section 3 summarizes the strategies used to develop  
97 various modules and the functions of each module, while Section 4 gives examples of the outputs  
98 of a historical dataset.

99

## 100 **2 Modeling algorithms**

101

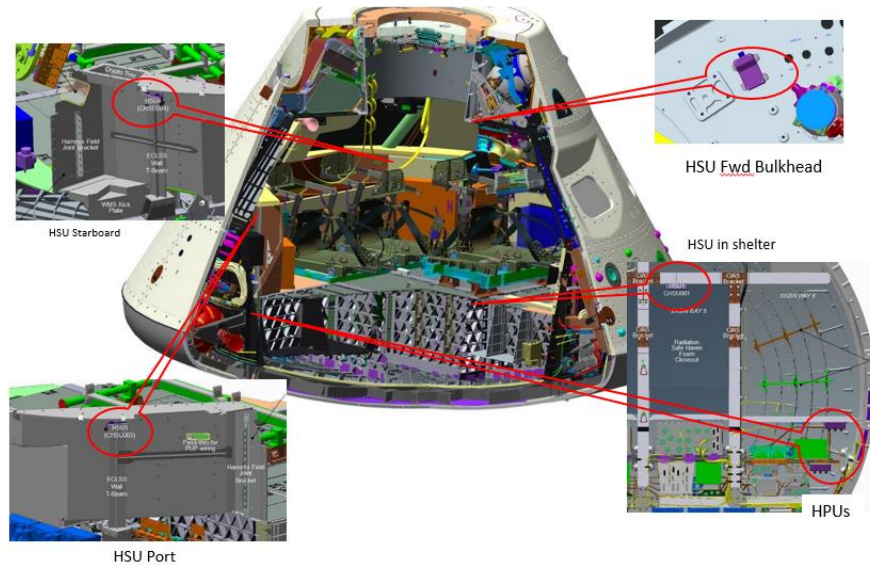
102 This section describes the algorithm of the two main components of ARRT. The method of  
103 estimating the ESPE organ doses from the vehicle dosimeter measurements is presented in  
104 section 2.1. A brief summary of the acute biological response model is given in section 2.2, the  
105 inputs of which come from the ESPE organ dose model.

106

### 107 **2.1 SPE organ dose estimation**

108

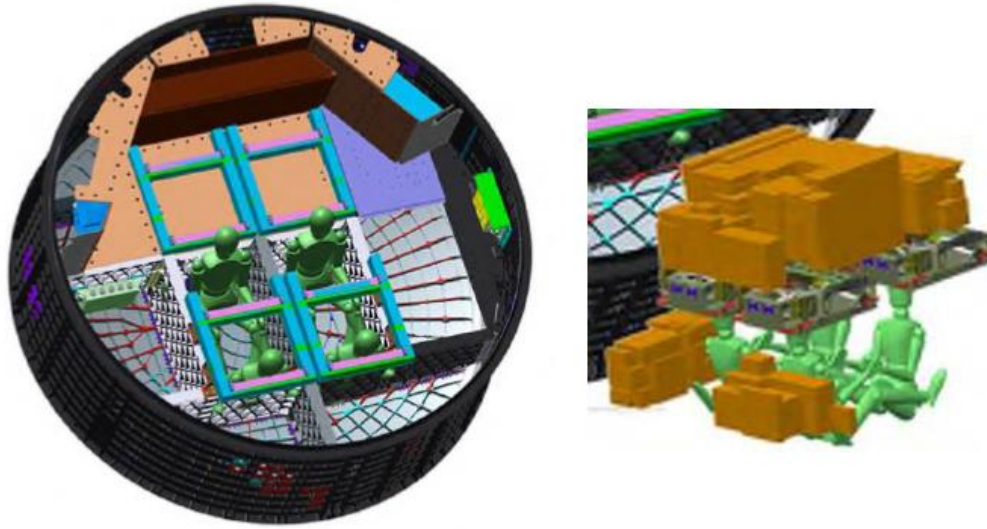
109 ARRT is developed specifically for the MPCV, an interplanetary spacecraft intended to carry a  
110 crew of four astronauts to destinations at or beyond LEO. The on-board radiation detection of  
111 this spacecraft will be provided by the Hybrid Electronic Radiation Assessor (HERA), which is a  
112 distributed dosimeter system based on the coupling of solid-state silicon detectors with the  
113 Timepix chips (Kroupa et al., 2015). In the upcoming Artemis I uncrewed flight, one HERA  
114 system with three detectors will be deployed at different locations. For Artemis II, the first  
115 scheduled crewed mission of MPCV, two HERA systems with six spatially separated sensors  
116 will be deployed for more robust measurement (Figure 1).  
117



118  
119 **Figure 1.** 6 HERA detectors at various locations of MPCV. HPU = HERA Processing Unit.  
120 HSU = HERA Sensor Unit.

121  
122 ESPE effects can be mitigated during the vehicle design process through thoughtful  
123 redistribution of mass to provide a secondary role in radiation shielding. The NASA Space  
124 Radiation Analysis Group (SRAG) has been closely involved with the design process of the  
125 MPCV to identify locations with lower inherent shielding and attempt to improve the overall  
126 shielding concept without adding excess mass to the vehicle. In addition to improving the design  
127 of the vehicle, a contingency location has been designated where the crew can shelter in the  
128 stowage bays of the vehicle, redistributing the mass contained within this area to improve  
129 radiation protection (Figure 2).

130



131

132 **Figure 2.** Schematic diagram of solar storm shelter for Orion MPCV after reconfiguration  
 133 (Courtesy of Lockheed Martin Inc.).

134 The algorithm of organ dose estimation from dosimeter measurement has been described in  
 135 detail in a previous paper (Mertens et al., 2018), which involves the following four major steps:

- 136 1. Generate a database of silicon doses at vehicle dosimeter locations and organ doses at the  
 137 normal crew seat locations as well as the crew locations inside the storm shelter, for 65  
 138 historical events with known total spectra.
- 139 2. Find the event in database that minimizes the differences between measured and database  
 140 averaged dose in silicon, whose spectrum thus best matches the spectral shape of the real-  
 141 time vehicle radiation environment.
- 142 3. Find the optimal scaling parameters between the vehicle dosimeter measurements and the  
 143 precomputed absorbed dose in silicon at the dosimeter locations for the selected event in  
 144 the historical ESPE database.
- 145 4. Apply the scaling parameters to the database of organ doses to obtain real-time organ  
 146 doses at the normal and storm-shelter crew locations.

147

148 The reliability of this algorithm was checked with the October 1989 event. Assuming an  
 149 isotropic distribution of ESPE protons, it was found that the differences are within 2% between  
 150 the total organ doses predicted by this algorithm and those calculated from the original spectrum  
 151 of this event, and the uncertainty of organ dose rates is on the order of 25–35% for the 329 time  
 152 intervals (30-minutes) (Mertens et al., 2018). This study also verified that the additional three  
 153 vehicle dosimeters in the Artemis II configuration do not improve the accuracy of the organ dose  
 154 prediction, but provide redundancy in the onboard measurements in case one or more of the  
 155 dosimeters malfunction. Nevertheless, for the Artemis I configuration, if one dosimeter  
 156 measurement is unavailable, the maximum difference of organ dose rates can reach 54% with  
 157 two dosimeter measurement, but the uncertainty can be less than 31% if HPU1 is among them. If  
 158 only one dosimeter is functioning, the error of using the dosimeter readings as organ dose rates  
 159 can be as high as 20-folds (Mertens et al., 2018).

160

161 2.2 Acute biological response models

162  
163 The prediction of acute biological responses to SPE exposure in ARRT is based on codes  
164 developed for ARRBOD and HemoDose (Kim et al., 2010; Hu et al., 2015). ARRBOD includes  
165 the neurovascular models (nausea and vomiting, fatigue and weakness) adapted from the RIPD  
166 models (Matheson et al., 1998), and four sets of hematopoietic models, which describe the  
167 dynamics of lymphocyte, granulocyte, leukocyte, and platelets in the peripheral blood after  
168 exposure (Hu et al., 2015). The HemoDose code is a biodosimetric tool that uses various blood  
169 cell counts after exposure to calculate absorbed doses, with a HemoGrade module linking acute  
170 and protracted doses with clinical severity scores of hematopoietic ARS, as well as the dynamics  
171 of hematopoietic stem cells in bone marrow (Hu, 2016). The user interface to these models has  
172 been modified for this work such that the Blood-Forming Organ (BFO) dose rates provided by  
173 the ESPE organ dose estimation algorithm are taken as inputs at every time point, and outputs  
174 are generated along with the real-time update of dosimeter readings.  
175

### 176 **3 ARRT development strategy**

177

178 This section describes the strategies used in developing various modules of ARRT, which  
179 include reading and plotting dosimeter recordings, detecting the onset and end of an event,  
180 calculating and plotting the relevant organ dose quantities, triggering the ARS biological models,  
181 and generating a flight note for FCT.  
182

#### 183 3.1 Reading and plotting dosimeter recordings

184

185 As meaningful real-time HERA data will not be available until Artemis I and Artemis II start  
186 their journeys in space, the development of ARRT must rely on a historical dataset and a real-  
187 time dataset.

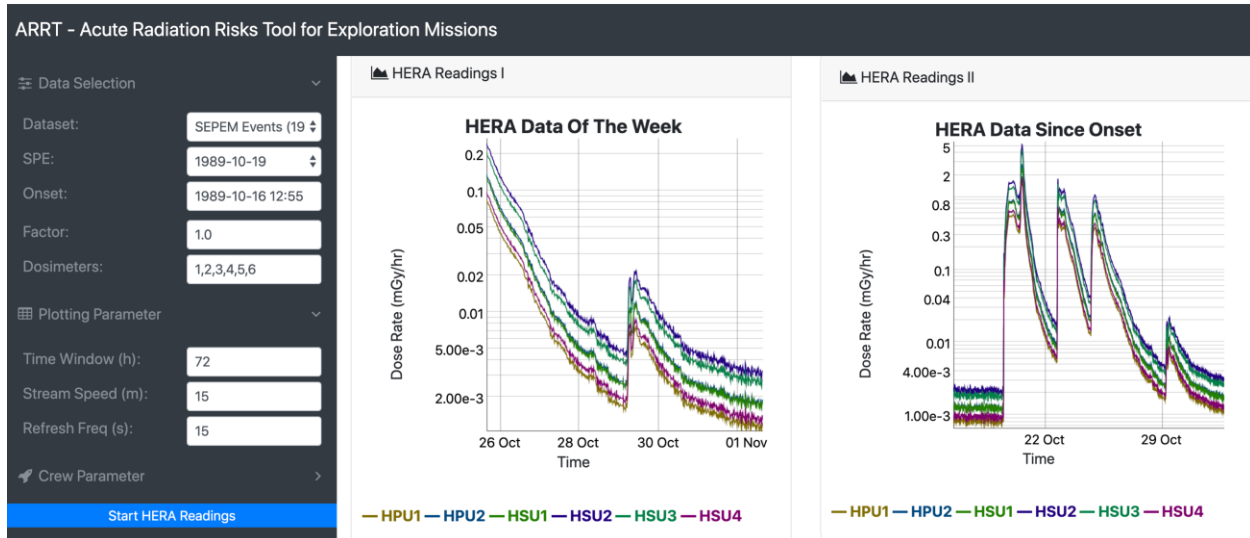
188 The historical dataset in ARRT is generated by transport calculation with the SEPTEM 2.0 dataset  
189 (<http://www.sepem.eu/>), which is a cross-calibrated uniform dataset using the Geostationary  
190 Operational Environmental Satellite (GOES) measured solar proton fluxes during 1974-2015,  
191 with an energy range 5-289 MeV. With segmental spectra (Hu et al., 2016) of 15-minute cadence  
192 generated from the fluxes as a boundary condition, and material and shielding thicknesses  
193 determined by ray tracing the computer-aided design (CAD) model of the MPCV for Artemis II  
194 (with 6 HERA sensors), transport calculations through the vehicle are performed by a numerical  
195 solution of the one-dimensional Boltzmann transport equation using the HZETRN2015 code  
196 (Slaba et al., 2016; Wilson et al., 2016). The resultant dataset contains dose rates for the 6  
197 dosimeters spanning uniformly from 1974 to 2015, with a 15-minute cadence.

198 At the time of this writing the web based ARRT is hosted on a Linux server inside the NASA  
199 JSC firewall, utilizing libraries such as dygraphs, PHP, JavaScript, Bootstrap, jQuery, HTML,  
200 and CSS. The simulated HERA dose rates for Artemis II configuration are stored locally with  
201 ARRT. It is assumed the Artemis I shielding configuration is the same as Artemis II, but with  
202 only 3 onboard dosimeters. The functions of reading and plotting of historical HERA data are  
203 conducted through interactive calls between codes developed in PHP, JavaScript and dygraphs.  
204 Figure 3 shows a snapshot how these interactions are performed, which is further illustrated in  
205 Section 3.5. After an event is selected in the SPE list, the onset time of the input panel is  
206 automatically set as the time 72 hours before the default onset of this event, and the HERA  
207 readings of the whole span of the event are plotted in the plot panel “HERA Reading II”, and the

208 7 days readings before the end of the event are plotted in “HERA Reading I”. The default values  
209 for “Factors”, “Dosimeters”, “Time Window”, “Stream Speed”, and “Refresh Frequency” are  
210 shown in Figure 3, which can be modified by the user. Dosimeters 1, 2, 3, 4, 5, 6 refer to HPU1,  
211 HPU2, HSU1, HSU2, HSU3, and HSU4, respectively. If one or more dosimeters malfunction,  
212 the user can delete the unit(s) and their readings will disappear from the plots.

213

214

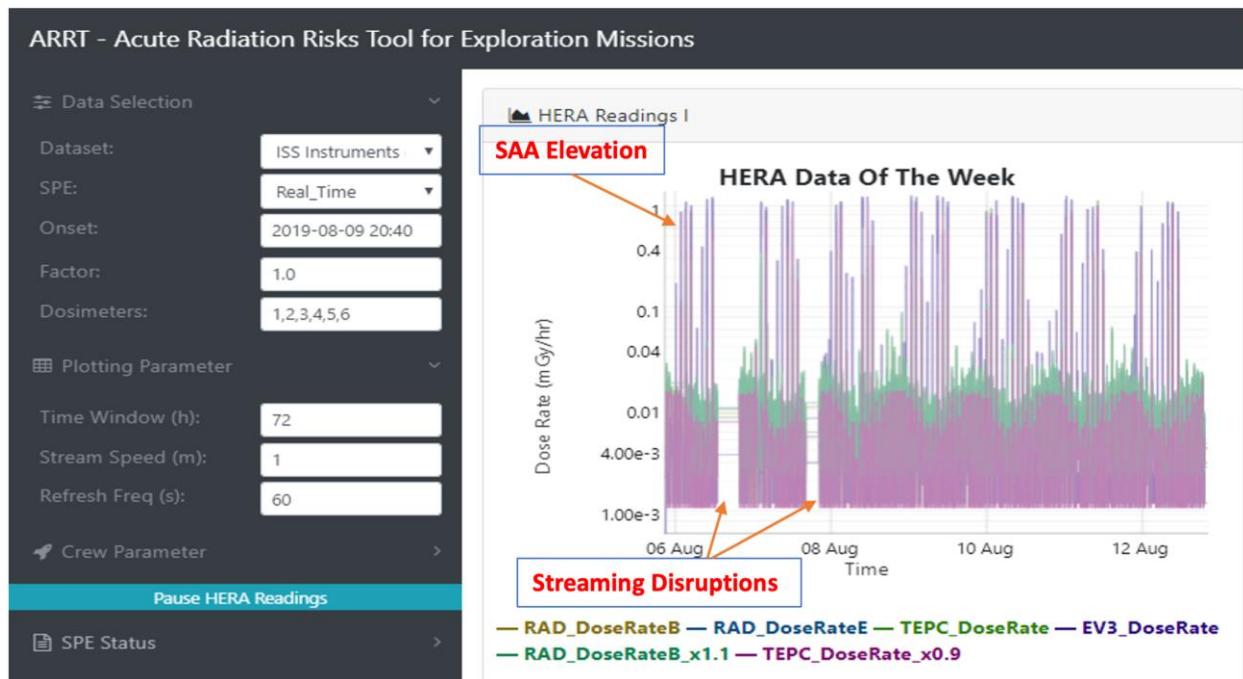


215

216 **Figure 3.** ARRT user input panel and HERA dose rate reading and plotting for historical SPEs

217 After the user clicks the “Start HERA Readings” button, both plots update at a pace set by the  
218 “Refresh Freq”. If the value of “Refresh Freq” is modified, the plotting will pause and need the  
219 user to click the “Resume HERA Readings” button to resume. If the value of “Time Window” is  
220 modified, the change will reflect in “HERA Reading II” in just one step, after that the value  
221 returns to the default 72 hours automatically. These two features were implemented to ease the  
222 usage for SRAG operations. All other modification of input values can be reflected and retained  
223 in the plots automatically. Changing the onset lets the user go to any time he/she may be  
224 interested in (within the SEPTEM range 1974-2015), increasing the factor can demonstrate the  
225 effects for large SPEs, while deselecting dosimeters allows the user to view readings of fewer  
226 HERA sensors. These functions are not needed for real-time operational monitoring, as the time,  
227 factor and the dosimeters are all set in such a situation. However, ARRT can be used as an  
228 analysis tool for events just passed, such as the example illustrated in Section 3.2, showing how  
229 these functions can be utilized. Additionally, the dygraphs library used in plotting allows  
230 zooming in the plots either horizontally or vertically, which is useful to examine the details of  
231 the measurement. At the bottom of each plot, there are two links for downloading data file and  
232 displaying data in a new tab, once the plot is activated.

233



235  
236 **Figure 4.** ARRT user input panel and HERA dose rate reading and plotting for the real-time  
237 data.

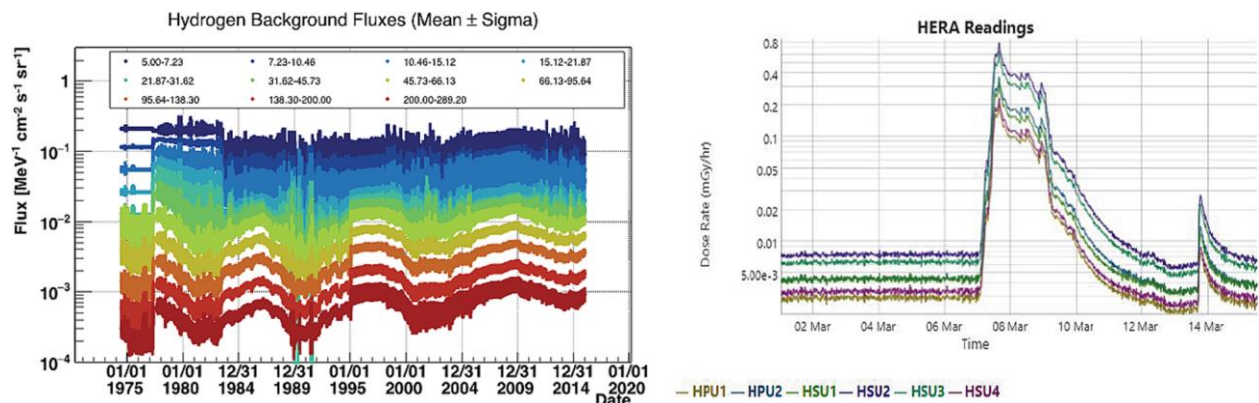
238 In addition to the SEPTEM dataset, ARRT uses a real-time dataset by linking with the databases  
239 of International Space Station (ISS) instruments maintained by SRAG, which include dose rates  
240 measured by Radiation Assessment Detector (RAD), Tissue Equivalent Proportional Counter  
241 (TEPC), and Extra-Vehicle Charged Particle Directional Spectrometer (EV-CPDS). The dose  
242 rates in the record uniformly populate ARRT from their starting service time to the present time,  
243 with a one-minute cadence. If the user selects the “RealTime” option as shown in Figure 4 and  
244 clicks “Start HERA Readings” button right after, the ISS dataset will be streamed and plotted in  
245 real time, updated every minute. As the ISS instrument data are downlinked to a SRAG internal  
246 database, from which ARRT retrieves the data, the streaming can be disrupted for various reasons.  
247 When this happens, ARRT automatically sets the readings of the units as the last available dose  
248 rates until the connection is restored. Figure 4 shows two such incidents between August 6 and  
249 August 8, 2019. As SRAG will maintain active instrumentation data for the future Artemis I and  
250 Artemis II missions in a similar manner as for ISS, the real-time onboard dataset can be easily  
251 migrated in ARRT.

252  
253 The real time data in Figure 4 are significantly different from the simulated historical data in  
254 Figure 3, because the radiation environments are different for current ISS and the GOES  
255 satellites. The ISS cruises mostly inside the Earth’s magnetosphere, with an average altitude of  
256 about 410 km; therefore, the majority of radiation sources from galactic cosmic rays and solar  
257 energetic particles are effectively sheltered, especially for those with low kinetic energies.  
258 However, the strength of the magnetic field is not the same along the trajectory, therefore the  
259 measured dose rates have large oscillations. In addition, the ISS passes through the South  
260 Atlantic Anomaly (SAA) region several times every day, causing significant dose rate elevation  
261 for 5~10 minutes each time (Figure 4). For the GOES satellites, because they orbit above the

262 Earth at geosynchronous altitude ( $\approx 6.6$  Earth radii, about 35,786 km), their geomagnetic effects  
 263 are very minor, and SAA has no impact. The planned trajectory of Artemis I will have the  
 264 vehicle orbiting the Earth and travelling through the van Allen belts before flying in free space to  
 265 the moon. The vehicle will then orbit the moon and return to Earth, passing through the free  
 266 space environment and the trapped radiation belts before landing. For the following Artemis II  
 267 and other human exploration mission with destinations beyond LEO, the spacecraft would have a  
 268 brief transit through the van Allen belts, mainly experiencing radiation environment in  
 269 interplanetary space. Therefore, the HERA readings of ARRT for future missions should be  
 270 more similar to the simulated historical data, without the oscillations and “spikes” as in Figure 4.  
 271

### 3.2 Detecting the onset and end of an event

273 Traditionally, the onset and end of an SPE are defined as the first and last time points of a period  
 274 with continually elevated proton fluxes higher than a threshold (Feynman et al., 1990; Jiggins et  
 275 al., 2012). However, because of the modulation of solar cycles, the background fluxes change  
 276 significantly from the solar minimum to the solar maximum (Figure 5), and the difference of  
 277 intra-vehicular dose rates can be as large as 2~3 times (Fig 3 in Norbury et al., 2019). If a fixed  
 278 dose rate were chosen as the threshold to determine the onset and end of an event, the first and  
 279 last time points of a same event (such as the one in Figure 5 (left panel)) would be different if it  
 280 occurred at different times in solar cycles. To avoid this problem, ARRT uses the background  
 281 dose rates as references for the threshold of an event, which are not fixed but varying along solar  
 282 cycles.  
 283  
 284



285  
 286 **Figure 5.** Variation of hydrogen background fluxes of SEP data (left) and HERA readings of  
 287 a typical SPE (right).

288  
 289 To automatically calculate the background dose rates is not always straightforward, especially  
 290 for the time period when multiple events occur sequentially. For the events plotted in Figure 5  
 291 (right panel), the background dose rate for the first event (with onset on Mar 07) is easy to  
 292 calculate, as any time window of any length before the onset can be selected, and the mean dose  
 293 rate is the correct background. However, for the second event (with onset on Mar 14), the time  
 294 window cannot be selected between Mar 07 and Mar 14, as the dose rates in this time period are  
 295 elevated by the first event. In ARRT, an algorithm is developed such that a one-week window is  
 296 selected to calculate mean dose rate and the number of points below the mean. If the number of

297 points with dose rates below the mean is less than 55% of the total number of points in this time  
298 window, it is certain that there are no SPEs during this window and the calculated mean is the  
299 background dose rate. Otherwise the time window shifts one week or additional weeks behind  
300 until the condition is satisfied. This algorithm has been tested for SEPTEM generated HERA  
301 readings and the calculated backgrounds are stable and independent from the occurrence of  
302 SPEs.

303  
304 For the historical dataset, the threshold for SPEs is defined as the two times the background dose  
305 rate, and the onset of an event is defined as a time point with two consequential dose rates above  
306 the threshold. Currently, for the real-time SPE, the definition of onset is the same, but the  
307 threshold has to be defined as 200 times the background, because a lower threshold would  
308 misinterpret the dose-rate elevation when ISS passes SAA as an SPE (Figure 4). As ISS travels  
309 inside the Earth's magnetosphere and no significant SPE has been recorded to date, we  
310 developed code to simulate a simple event with specific starting time, hours to the peak, hours to  
311 the end, and a factor that times the original data. With these virtual events, ARRT can check if  
312 the real-time data works for the organ dose fitting module and acute risk modeling module.  
313 Figure 6 shows such an event starting at 2019-04-15 00:00, with 1 hour to the peak, 240 hours to  
314 the end, and 500 times of the original readings at the flux peak. Because the code modifies the  
315 readings with a simple linear rising from background to peak, and the threshold is defined as 200  
316 times of the background, the detected onset of this event is 2019-04-15 00:28, as shown in Figure  
317 6. Before the onset, the "SPE Status" is in a "Nominal" mode with a green light. When the data  
318 reading reaches the onset, ARRT enters an "Event in Progress" mode with a red light in "SPE  
319 Status" (Figure 6), the time value in the "Onset" box becomes fixed, and the "Time Window"  
320 value keeps increasing at a pace set by the "Stream Speed" and "Refresh Freq". In the meantime,  
321 the plot in "HERA Reading II" shifts its origin to the onset, displaying the readings sequentially  
322 since onset, while the plot in "HERA Reading I" continues streaming with time for one week's  
323 readings. This "Event in Progress" mode works similarly for the 159 recorded SPEs in historical  
324 dataset, but with different thresholds.



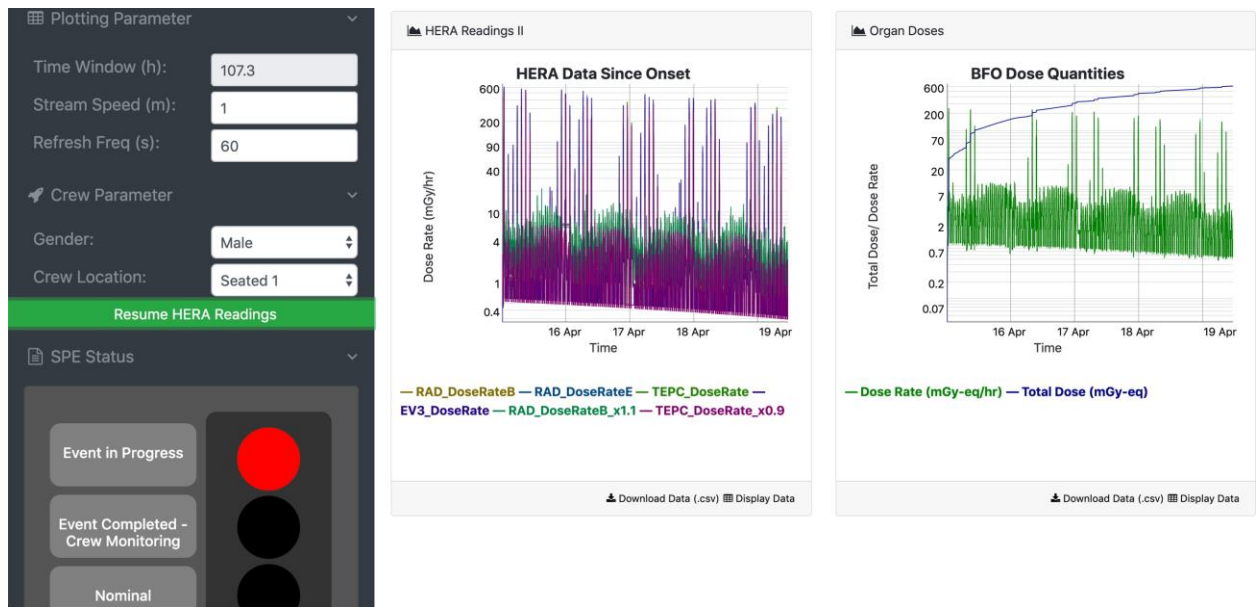
325  
326 **Figure 6.** “Event in Progress” mode for a virtual event with the real-time dataset.

327 As reported by other researchers (Feynman et al., Tylka et al., Jiggins et al., 2012), many  
328 consecutive events are not independent in time, and a minimum dwelling time parameter (e.g.,  
329 24 hours in Jiggins et al. 2012) is needed so that they could be treated as the same event. Based  
330 on SRAG’s operational guidance, ARRT chooses a two-hour dwelling time to determine if  
331 consecutive events can be treated as different events, and the end of an event is defined as a time  
332 point following two hours of dose rates below the threshold, for both the historical and real-time  
333 datasets. When the end is reached, ARRT goes back to “Nominal” mode with a green light in  
334 “SPE Status”, the time value in the “Onset” box changes to an unfixed onset, and the “Time  
335 Window” value returns to the default 72 hours, accompanying with the changes in the plots in  
336 nominal mode. As all effects of the previous event is reset once it reaches the end, there is a  
337 health risk issue if the event is big enough to induce ARS. To remedy this problem, a dose-  
338 dependent monitoring time parameter is introduced using the following formula:

$$339 \text{ monitoring time (hours)} = 24.0 * (\text{total dose (mGy-eq)} / 50.0)$$

340  
341  
342 For events with total BFO dose > 250 mGy-eq, which is the threshold of ARS induction for  
343 terrestrial radiation, the health effects will be monitored at least 5 days. For these rare large  
344 events, when the end is reached, ARRT goes to a “Crew Monitoring” mode with a yellow light  
345 in “SPE Status”, and the time values in the “Onset” box and “Time Window” box are maintained  
346 as in “Event in Progress” mode until this monitoring period finishes. In this way, the impacts of  
347 big events to the health of crew are preserved for complete analysis. An example for this  
348 treatment will be discussed below, to demonstrate how large consecutive events can be analyzed  
349 correctly.

350  
351 **3.3 Calculating and plotting organ dose quantities**

353  
354

**Figure 7.** Plot of organ dose calculation for a male astronaut at “Seated” location 1.

355 Whenever an SPE is detected, a set of code is launched to project organ doses from dosimeter  
 356 measurement. This is a complicated process with each step involving spectral matching in a  
 357 precomputed dose database, scaling factors fitting between the vehicle dosimeter measurement  
 358 and the precomputed dose quantities of the matched event, and linear scaling of the precomputed  
 359 organ dose quantities (Mertens et al., 2018), which is summarized in Section 2.1. The output of  
 360 each step of calculation include 27 organ doses at 8 locations in MPCV (4 nominal seats and 4  
 361 sheltered seats), for male and female astronauts respectively (Mertens et al., 2018). To reduce the  
 362 amount of computation for this step, two input parameters are introduced, i.e., the “Gender” and  
 363 the “Crew Location”, allowing the user to check some subtle variations for different genders and  
 364 locations in different runs. Figure 7 shows the output of a calculation for a male astronaut at  
 365 “Seated” location 1 of the virtual event with onset on 2019-04-15 00:28, which was paused at  
 366 107.3 hours after onset. The organ dose plot includes 107.3×60 BFO dose rates and accumulative  
 367 doses since the onset of the event, as the cadence is 1 minute.

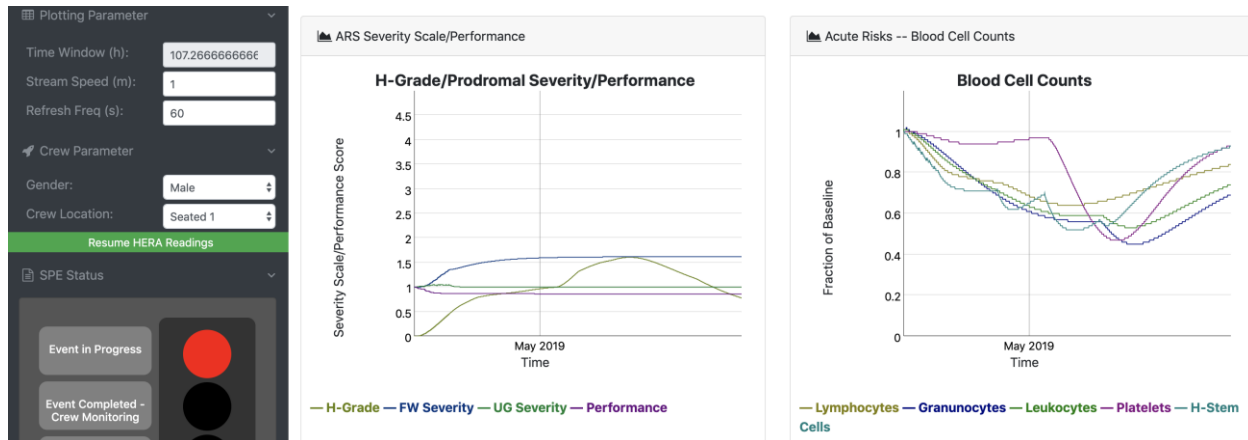
368

369 As ARRT is a real-time operational tool for the exploration missions, all calculations are  
 370 required to finish along with the streaming of dosimeter reading. For the real-time data such as  
 371 those showing in Figure 7, all 107.3×60 steps of organ dose computation are required to finish  
 372 within one minute (the cadence of data streaming). We found this could not be done with  
 373 sequential code, or by breaking the code into sections with each conducting a small number of  
 374 times calculation, or by parallelizing the code to use all nodes simultaneously. The solution was  
 375 found by running the sequential code just in the background of the Linux system, and an  
 376 unlimited number of processes are spawned to the backend cluster at a same time. The speed of  
 377 calculation in this way is the fastest among all trials. However, for longer duration events, the  
 378 calculation will cause a delay in the update of the plots, as additional time is needed to plot 1-  
 379 week HERA data, to plot HERA data since onset, to perform ARS calculation and plotting, and  
 380 to generate flight notes. If this is the case, the user can increase the “Stream Speed” and the  
 381 corresponding “Refresh Freq” inputs to allow longer gaps between reading dosimeter data, i.e.,  
 382 by manually increasing the default cadence, so that all tasks can be finished properly within the

383 cadence. For historical SEPTEM dataset, such problems are not presented as the cadence is 15  
384 minutes and long enough to conduct the required computations even for the event of longest  
385 duration. At the time of this writing, the Linux server hosting the code has only 32 CPUs. Once  
386 the code is migrated into a server with more CPUs, the speed limit should be lifted.  
387

### 388 3.4 Triggering the ARS biological models

389



390  
391 **Figure 8.** Plot of ARS projections for a male astronaut at “Seated” location 1, if encountering a  
392 virtual event depicted in Figures 6 and 7.

393 Early radiobiological studies suggested all ARS symptoms are deterministic effects that manifest  
394 only above a threshold (NAS, 1976). For example, the widely used RIPD software set 0.5 Gy as  
395 the threshold to trigger two neurovascular models (Matheson, 1998). However, later  
396 investigations indicated the damages to the radiosensitive systems have no threshold limit; at low  
397 dose levels, these changes may be localized or transient, and/or they may be repaired; at high  
398 dose radiation, they may be more widespread, severe and persistent (Fliedner, et al., 2001).  
399 Therefore, ARRT does not set a threshold for the incorporated ARS models, but generates results  
400 of various endpoints whenever an ESPE occurs.  
401

402 For the virtual event described above, the total BFO dose is about 600 mGy-eq for a male  
403 astronaut at “Seated” location 1 after 107.3 hours’ exposure (Figure 7). Figure 8 shows various  
404 ARS effects that ARRT projects, from the onset of the event to up to 42 days (1000 hours) after  
405 the onset. The left plot displays ARS severity and performance prediction, updated in every step  
406 of real-time data reading (i.e., 1 minute). This includes H-grade (HemoGrade), severity scale of  
407 UG (upper-gastrointestinal) and FW (fatigue and weakness) symptoms, and PD (performance  
408 decrement). HemoGrade is modeled based on the changes of peripheral blood cell counts after  
409 radiation exposure (Hu, 2016). It indicates the extent of damage to hematopoiesis and the  
410 corresponding prognosis for autologous recovery, and it can be used to suggest optimal  
411 therapeutic treatment (see Table 1). UG and FW symptoms are outputs of two neurovascular  
412 models adapted from the RIPD models (Matheson, et al., 1998), describing severity of nausea  
413 and vomiting, fatigue and weakness in numerical scales (Table 2). Performance is defined as the  
414 baseline time for a healthy crew to complete a task divided by the time taken to complete the task  
415 when ill. Calculation of PD is based both on the severity of symptoms and the mental/physical  
416 difficulty of the crew’s assigned tasks. A PD greater than 0.75 is considered “Effective”, 0.25 to  
417 0.75 is “Performance Degraded” and below 0.25 is “Ineffective” (Matheson, et al., 1998). For the

418 virtual event at around 107.3 hours since onset, the HemoGrade steadily increases from 0 to 1  
 419 during the first week, stays at level 1 for the second week, then increases to peak at 1.5 and  
 420 decreases to 1 during the third and fourth weeks, and maintains at level 1 till the 42 days (Figure  
 421 8), indicating mild to moderate injury to the hematopoietic system with certain autologous  
 422 recovery (Table 1). The FW score increases to 1.5 for the first week after onset, and maintains at  
 423 the level till 42 days, while UG and performance results show minimal or no impact at this level  
 424 of exposure (Figure 8 and Table 2).  
 425

426 **Table 1.** Textual descriptions of the HemoGrade severity level and prognosis and therapeutic  
 427 options

<b>Grading</b>	<b>Extent of impairment</b>	<b>Prognosis</b>	<b>Therapeutic options</b>
H0	No damage	No observable symptoms	No need for hematopoietic treatment
H1	Mild damage	Autologous recovery certain without critical phase*	No need for hematopoietic treatment
H2	Moderate damage	Autologous recovery certain with low risk critical phase	Blood component therapy if indicated by bleeding, or appropriate antibiotic agents to cope with bacterial infections
H3	Severe damage	Autologous recovery certain with high risk critical phase	Same as those in H2. Additionally cytokines/growth factors should be administered as early as possible
H4	Fatal damage	Autologous recovery most unlikely	Stem cell transplantation, supplemented by all other supportive hematopoietic treatment

428 \*Critical phase is defined as the duration with constant cell counts below the normal range, resulting high or  
 429 low risks of developing bleeding or infectious diseases.  
 430

431 **Table 2.** Textual descriptions of the symptom severity level of prodromal radiation sickness

<b>Severity Level</b>	<b>Nausea/Vomiting</b>	<b>Fatigue/Weakness</b>
1	No effect	No effect
2	Upset stomach, clammy and sweaty, mouth waters	Somewhat tired, with mild weakness
3	Nauseated, considerable sweating, swallows frequently to avoid vomiting	Tired, with moderate weakness
4	Vomited once or twice, nauseated, and may vomit again	Very tired and weak
5	Vomited several times, including the dry heaves, severely nauseated, and will soon vomit again	Exhausted, with almost no strength

432  
 433 The right plot in Figure 8 describes the modeled dynamics of various blood cell counts at this  
 434 scenario, which are expressed as ratios to their baseline counts. These are generated by the four  
 435 hematopoietic models used in the HemoDose software (Hu et al., 2015). In addition to the counts  
 436 of lymphocytes, granulocytes, leukocytes, and platelets from the onset to the 42 days , the time

437 course of the number of hematopoietic stem cells is also reported as one endpoint of the models  
438 (Hu et al., 2012), which is an indicator of the possible autologous recovery of this system  
439 (Fliedner et al., 2002). All these outputs are updated at each step of dosimeter data reading (i.e.,  
440 1 minute), along with the calculation of ARS severity scale and performance, giving updated  
441 information of the possible health outcomes of the crew and providing instant guidelines to the  
442 ground FCT. However, it is not certain if a hematological analyzer will be onboard in future  
443 exploration missions. If such a device is available, the cell counts in peripheral blood can be used  
444 to verify the projected dose as the HemoDose tool does (Hu et al., 2015). In addition, they can  
445 serve as real time biomarkers to assess ARS and develop clinical guidelines. An additional merit  
446 of the plots in Figure 8 is the projection of the critical phase, which is defined as the duration  
447 with constant cell counts below the normal range, resulting high or low risks of developing  
448 bleeding or infectious diseases. For the virtual event, the calculation indicates such phase may  
449 appear during the third and fourth weeks after the onset, giving plenty of time for the ground  
450 FCT to make decision if any medical intervention as listed in Table 1 is needed (Hu, 2016).  
451 Because SPEs can be effectively shielded, and current vehicle designs incorporate smart  
452 shielding concepts such as the redistribution of vehicle mass in MPCV, with an effective  
453 warning system for a large SPE to reduce the event exposure, it is very unlikely that astronauts  
454 inside an interplanetary spacecraft like MPCV will experience such severe health impacts that  
455 need these medical interventions (Hu et al., 2020).  
456  
457

**Space Weather Conditions:**

An ESPE was observed at 2019-04-15 00:26:00 as defined by [Flight Rule]. The mission average background dose, as monitored by HERA, is 7.10E-3 mGy/hr. As of 2019-04-19 11:46:00, the average dose rate is 3.93E+0 mGy/hr.

**Recommended Crew Actions:**

Based on the projected short-term crew impacts (see below) the crew is recommended to perform the Radiation Event Cabin Reconfiguration protocol and seek shelter in the storage bays per [Flight Rule].

**Short-Term Crew Impacts (48 hours):**

On-board instrumentation indicates that as of 2019-04-19 11:46:00, total exposure due to this ESPE was 6.90E+2 mGy. According to model predictions, a total bone marrow exposure of 6.27E+2 mGy-eq is projected. At this level, per [Flight Rule], Acute Radiation Syndrome *is a concern for the crew*. Symptoms such as nausea and anorexia may appear within 24 hours of exposure, manifested as an upset stomach with clammy/sweaty skin and watering mouth. Complete disappearance of these symptoms is certain within 48 hours of exposure. Fatigue and mild weakness may appear during this time period. Bloodwork will indicate a mostly asymptomatic decrease in lymphocyte concentration.

The following crew impacts are expected over the next 48 hours since the onset of the ESPE\*:

Symptom	2h	4h	6h	12h	18h	24h	30h	36h	42h	48h	Incidence (%95CI)
Nausea/Vomiting	1.00	1.00	1.00	1.01	1.02	1.02	1.01	1.03	1.03	1.03	0.00 (4.47,0.00)
Fatigue/Weakness	1.00	1.00	1.00	1.00	1.00	1.01	1.01	1.03	1.05	1.07	11.04 (45.17,1.00)
Performance Decrement	1.00	1.00	1.00	0.98	0.97	0.96	0.96	0.93	0.92	0.91	N/A
HemoGrade	0.00	0.00	0.00	0.00	0.01	0.02	0.04	0.06	0.09	0.11	N/A

\*Check the reference tables for the definitions of the symptom severity levels, incidence, performance decrement, and HemoGrade.

**Continuing Crew Impacts (2 days - 6 weeks):**

Fatigue and weakness may persist for several weeks. The crew are at low risk of developing infectious diseases or bleeding due to a decrease in concentrations of lymphocytes, platelets, and granulocytes below the lower end of the normal range. Autologous recovery is certain.

458  
459  
460  
461  
462  
463  
464  
465  
466  
467  
468  
469  
470  
471  
472  
473

**Figure 9.** Flight note for a male astronaut, if encountering a virtual event depicted in Figures 6 and 7.

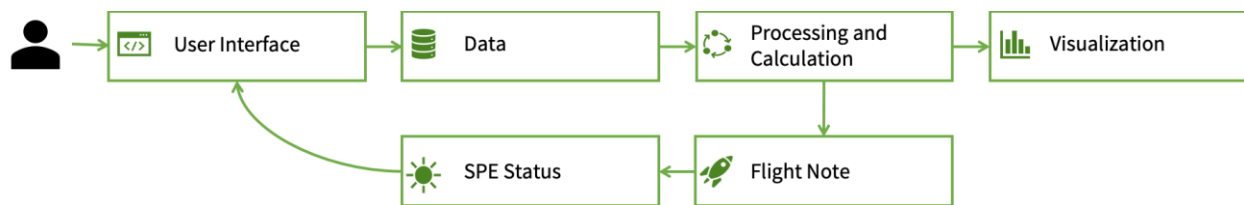
3.5 Generating a flight note for ARS management

As described above, MPCV is designed with an integrated shelter. If there is a possible risk to crew health, the crew will be asked to perform the Radiation Event Cabin Reconfiguration (RECR) protocol and seek shelter in the storage bays. Generally crew shelter can be assembled in 30 minutes, and the crew can safely remain in the shelter through the event, leaving briefly as approved to conduct mission critical or hygiene-related tasks. As one of the console operators' suite of tools, ARRT will be initiated at launch and run consistently in the background. Once an ESPE is detected, the radiation console will be notified automatically and the ARS projections will be performed. This information will be used to automatically generate a Flight Note for communication with FCT, all recommendations being worked through the Flight Surgeon.

474 Figure 9 displays a sample flight note for a male astronaut if encountering a virtual event  
 475 depicted in Figures 6 and 7. The note contains information on space weather conditions,  
 476 recommended crew actions, short-term crew impacts (48 hours), and continuing crew impacts (2  
 477 days – 6 weeks). Except for the space weather conditions, all other information is generated  
 478 based on the results of ARS modeling calculation. The thresholds to recommend crew action and  
 479 ARS concerns are both set as 100 mGy-eq, and that for short-term crew impacts is set as 250  
 480 mGy-eq. The texts of symptoms description and recommendation are categorized into 8  
 481 scenarios based on the calculated total BFO dose from the organ dose estimation code  
 482 (Supporting Information), which can be changed as the ESPE progresses in time. The table listed  
 483 in flight note gives numerical scores for NV, FW, PD, and H-grade over the first 48 hours since  
 484 onset, as well as incidence of the two neurovascular effects. Like the ARS plots, all texts in flight  
 485 note are updated at every time step of dosimeter reading and can be downloaded in Microsoft  
 486 Word format. If no increase in dose over threshold, only space weather conditions will appear in  
 487 flight note, with mission background dose rate and the average dose rate of the present time, and  
 488 the note download link is inactive.

### 489 3.6 Software Structure of ARRT

490 ARRT was developed with many state-of-the-art facilities for full stack web development, with  
 491 its overall workflow depicted in Figure 10. The user interacts with an interface to set parameters  
 492 of the query (i.e. time window, stream speed, etc.). Then the application loads the appropriate  
 493 dataset, processes the data to check if ESPE threshold is reached, in the meantime to visualize  
 494 the data and to generate flight note. Certain levels of ESPE result in additional calculations,  
 495 expanded visualizations, and detailed flight notes all of which happen seamlessly by modifying  
 496 SPE status and input parameters automatically (Figure 10). Regardless of the existence of an  
 497 ESPE, the modules corporately run execute continuously unless if the user clicks the “Pause  
 498 HERA Readings” button (Figures 4 and 6).



499  
 500 **Figure 10.** The overall workflow of ARRT web application.

## 501 4 ARRT operation for a typical event

502  
 503 The occurrence of ESPEs is hard to predict, and their developing patterns are vastly different.  
 504 Table 3 lists 20 biggest events occurred between 1974 and 2015, calculated from SEPTEM 2.0  
 505 dataset (<http://www.sepem.eu/>). It is clear that every event is unique, in term of total dose, dose  
 506 rate at peak, duration, as well as the waiting time. Additionally, the time for dose rates to reach  
 507 the peaks, and the time parameters for accumulative doses can be different as large as over two  
 508 magnitude. To be able to process the diverse features of the events, the ARRT code should be  
 509 flexible enough to deal with different scenarios, but in the meantime be robust to generate the  
 510 correct results in an automatic manner. Additional challenges exist for multiple events occurring

511 in a short time period. To make the outcome of ARS prediction more relevant for the console  
 512 operational team, it is not always easy to decide whether to treat sequential events separately or  
 513 inter-dependently. The robustness of ARRT has been tested with all the simulated HERA  
 514 readings from SEPEM 2.0 dataset, and for all of the 159 significant events, ARRT can correctly  
 515 read and plot the data, project organ doses and ARS risks, and generate flight notes consistent  
 516 with the numerical results. In the following an event with multiple sub-events is used to  
 517 demonstrate how ARRT is smart to treat sequential events correctly.

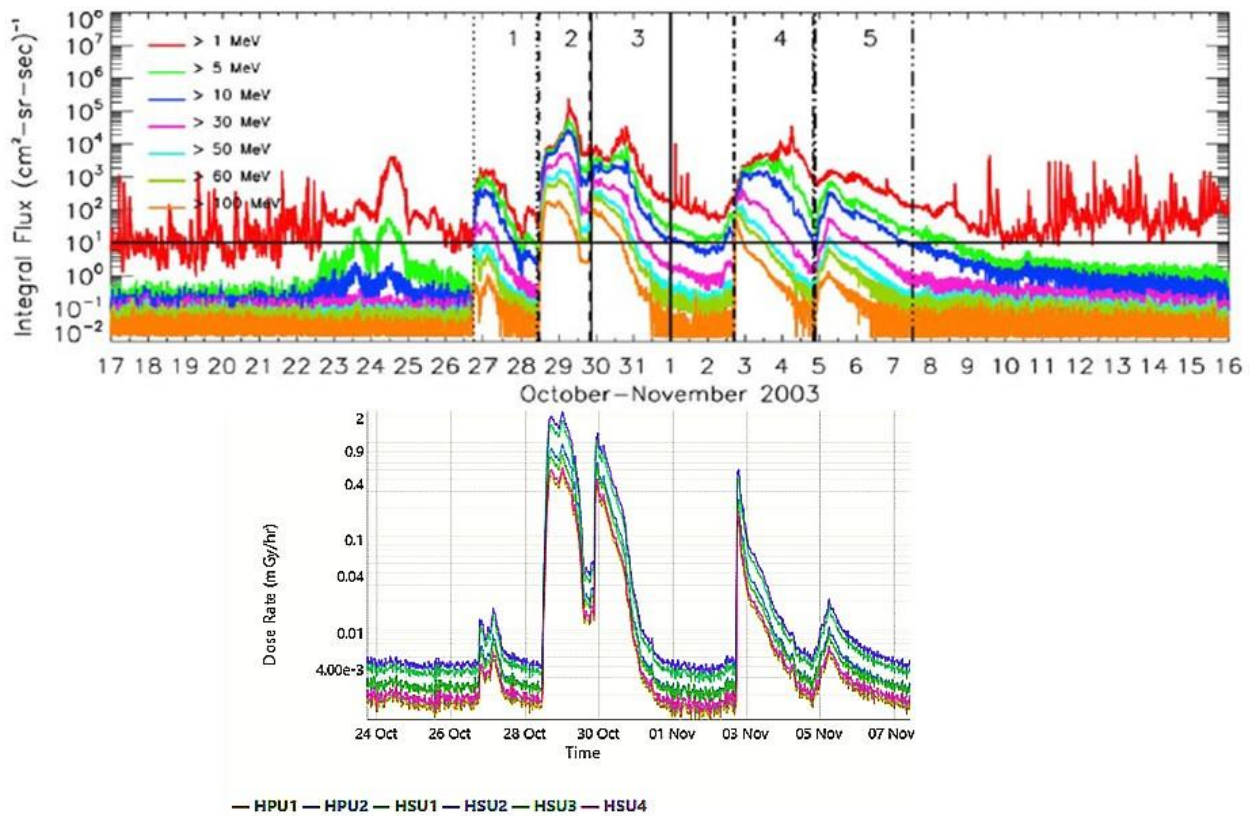
518  
 519

**Table 3.** 20 biggest ESPEs during 1974-2015\*

SPEs	Start Time	Dose (cGy)	DR <sub>Peak</sub> (cGy/h)	Duration (h)	T <sub>peak</sub> (h)	T <sub>10</sub> (h)	T <sub>50</sub> (h)	T <sub>90</sub> (h)	T <sub>waiting</sub> (d)
1	1989-10-19 12:55	2.18e+01	1.15e+00	316.0	26.5	10.2	30.2	134.5	10.1
2	2000-07-13 09:25	1.32e+01	3.75e-01	153.0	48.2	27.2	32.8	49.2	31.9
3	2000-11-08 23:40	1.06e+01	9.54e-01	105.5	4.2	2.8	7.8	17.0	23.0
4	2003-10-26 17:55	9.74e+00	4.71e-01	281.2	54.5	46.8	56.8	89.8	148.1
5	1989-09-29 11:25	9.17e+00	5.73e-01	239.8	8.5	4.2	12.2	29.5	36.1
6	2001-11-04 16:25	6.49e+00	6.65e-01	111.2	34.0	5.5	29.8	36.8	11.5
7	2005-01-16 01:25	6.37e+00	2.11e+00	174.0	101.8	51.0	103.2	112.5	63.5
8	2012-03-07 02:10	4.08e+00	1.87e-01	195.5	13.2	11.2	25.2	47.8	35.8
9	1991-05-31 09:25	3.24e+00	1.11e-01	445.0	269.2	172.0	271.5	371.5	17.1
10	2001-04-15 13:55	2.73e+00	5.11e-01	118.0	1.2	1.2	4.0	65.8	2.1
11	2006-12-06 12:40	2.65e+00	5.26e-02	222.5	23.5	23.8	160.0	168.5	446.1
12	1989-08-12 15:55	2.36e+00	1.05e-01	282.2	85.2	11.5	86.0	119.0	17.1
13	1992-10-30 19:10	2.12e+00	2.45e-01	142.8	58.8	11.2	62.0	74.0	123.3
14	2001-09-24 11:40	1.94e+00	8.61e-02	141.5	20.2	11.8	23.0	39.0	36.0
15	1997-11-04 06:40	1.72e+00	3.39e-02	127.5	71.0	56.0	61.2	73.8	745.2
16	1981-10-08 00:40	1.42e+00	4.36e-02	235.2	114.2	104.0	120.5	144.0	78.3

17	1990-05-21 22:40	1.30e+00	3.86e-02	231.8	6.5	6.5	87.8	168.5	22.6
18	2002-04-21 01:40	1.20e+00	6.25e-02	115.5	8.8	3.8	12.2	31.8	106.2
19	1991-03-23 07:25	1.08e+00	2.38e-01	164.2	20.5	12.5	19.0	22.0	49.1
20	2005-09-07 21:55	1.00e+00	2.14e-02	205.0	46.2	19.0	44.2	69.2	13.5

520 \*Based on calculation with HZETRN2015 for silicon dose rates inside a 10 g/cm<sup>2</sup> sphere in interplanetary space, by  
521 using spectra of every 15 minutes data from SEP-EM 2.0 dataset (<http://www.sepem.eu/>). The onset and end times  
522 are defined similar to this paper, except for the dwelling time (24 hours). T<sub>peak</sub>, T<sub>10</sub>, T<sub>50</sub>, and T<sub>90</sub> are time parameters  
523 (hours) for dose rates reaches the peak, and accumulative dose reaches 10%, 50%, 90% of the total dose of the  
524 event, while T<sub>waiting</sub> is the time (days) between the end of the previous one to the onset of the present one.  
525



526  
527 **Figure 11.** GOES-11 proton flux measurement of 2003-10-26 ESPE (top, adapted from Mertens  
528 et al., 2010) and ARRT simulated HERA readings (bottom).  
529

530 The 2003 Halloween storm is a typical ESPE with multiple events lasting for more than 10 days,  
531 which ranks No. 4 among the biggest events during 1974-2015 (Table 3). The proton fluxes  
532 recorded by GOES detectors indicate 5 sub-events nearly overlapping with each other (Figure  
533 11) [Mertens et al., 2010], whose onset and end times are listed in Table 4 according to different  
534 definitions. The NOAA parameters are estimated by using the proton data archived at NOAA's  
535 National Center for Environmental Information  
536 (<http://www.ngdc.noaa.gov/stp/satellite/goes/index.html>), which defines the start of an SPE as

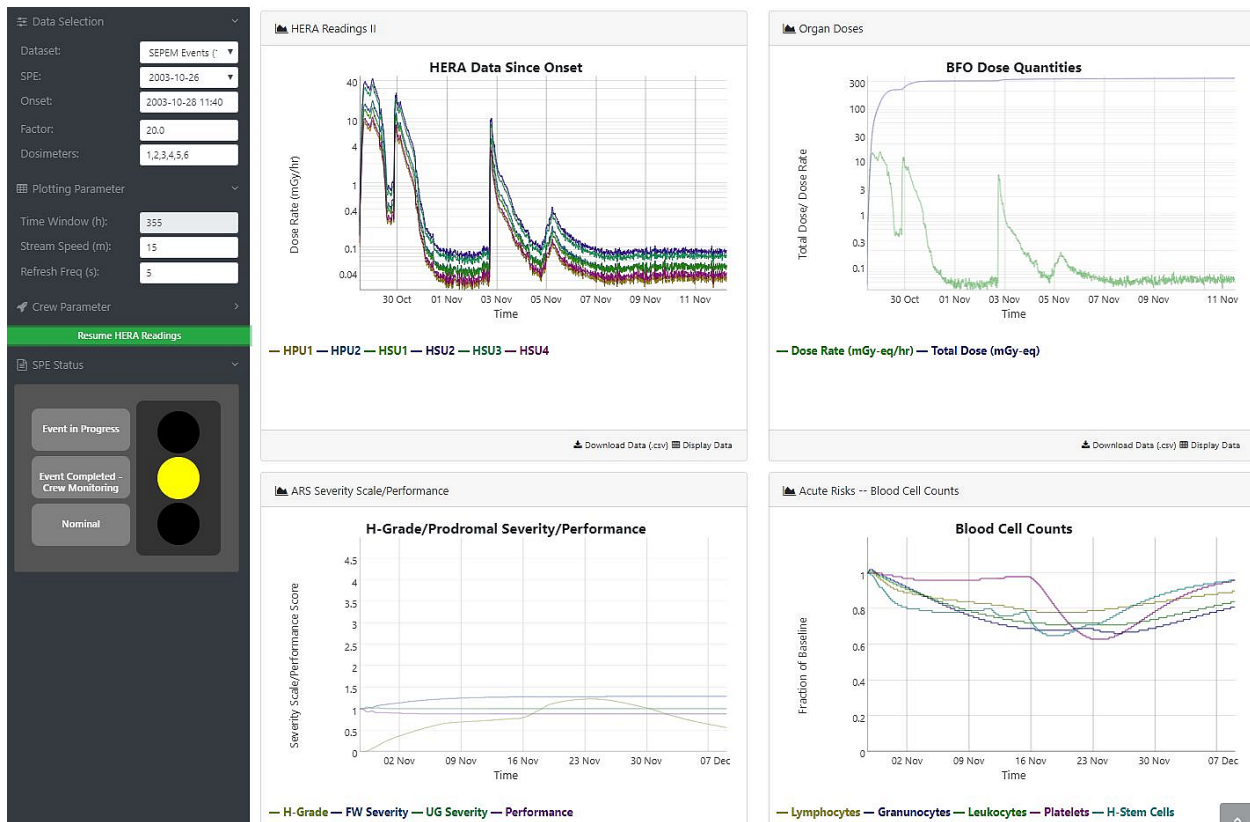
537 when the >10 MeV integral proton flux exceeds 10 proton flux units ( $\text{pfu} \equiv \text{cm}^{-2}\text{sr}^{-1}\text{s}^{-1}$ ) in three  
 538 consecutive 5 min periods, and the end as the last time the flux was greater than or equal to 10  
 539 pfu [NOAA, 2009]. As the fluxes of >10 MeV protons between events 2 and 3 are not below the  
 540 threshold (Figure 11), they should be considered as one event by this definition. As discussed  
 541 above, ARRT's definition is based on the elevation of HERA dose rates within the MPCV.  
 542 Because the contribution to silicon dose behind the spacecraft shielding comes mainly from  
 543 protons in energy range 100-300 MeV, the onset and end times estimated by ARRT are  
 544 substantially different from NOAA's. The dwelling time between event 2-3 and event 4 is about  
 545 24 hours with NOAA's definition, but increases to 58.5 hours with ARRT's definition (Table 4).  
 546

547 **Table 4.** Onset and end times for the sub-events of 2003 Halloween storm.

Sub-events	NOAA onset	NOAA end	ARRT(1)* onset	ARRT(1)* end	ARRT(20)** onset	ARRT(20)** end
1	10-26 18:35	10-27 19:40	10-26 18:10	10-27 10:25	10-26 18:10	10-27 10:25
2-3	10-28 12:25	11-01 10:50	10-28 11:40	10-31 07:10	10-28 11:40	-
4	11-02 11:05	11-04 19:40	11-02 17:40	11-04 10:25	-	-
5	11-04 22:35	11-07 12:25	11-05 00:10	11-05 17:55	-	11-12 18:55

548 \*The factor of ARRT run is 1. \*\*The factor for ARRT run is 20.

549  
 550 If the factor of ARRT run is 1, i.e., no enhancement applied to the original data, treating these  
 551 events separately causes no issues for health risk analysis, as the BFO doses for these four events  
 552 are 0.08, 15.5, 1.25, and 0.11 mGy-eq, respectively, all far below the threshold to trigger ARS  
 553 response (i.e., 250 mGy-eq). However, if a factor of 20 is applied (for post-event analysis), the  
 554 events 2-3 will generate a BFO dose of 310 mGy-eq for astronauts inside MPCV, which will  
 555 induce ARS that may last 4-6 weeks (Figure 8). As events 4 and 5 will add significant doses and  
 556 deteriorate the ARS in this scenario, they should be included in risk estimation together with  
 557 events 2-3. There are different ways to include sub-events in an episode (Robinson et al., 2018).  
 558 One simple way is to extend the dwelling time if an event reaches the threshold, and the length  
 559 of the dwelling time depends on the size (i.e., dose) of the event, which is how ARRT adapts.  
 560 This dose-dependent dwelling time is better than one with a fixed length, as the dwelling time  
 561 (waiting time) varies significantly for different events (Table 3). Applying the threshold is  
 562 important in the algorithm, as otherwise any event will lead the tool into a "Crew Monitoring"  
 563 mode for a certain time, which is unnecessary if the threshold is not reached. The quantitative  
 564 relationship of the dose dependence is also essential, which needs to extend the dwelling time to  
 565 the time window relevant to ARS risks for significant exposure. Furthermore, the exposure  
 566 induced by the following events needs to be taken account in real time, so that the duration can  
 567 be further extended when total dose of the episode increases. All these considerations have been  
 568 implemented seamlessly in the code of the flight note module which detects and determines the  
 569 onset and end of an event.  
 570



571  
572 **Figure 12.** An ARRT run with a factor of 20 for 2003 Halloween storm. The HERA reading was  
573 paused near the end of the combined events 2-5.  
574

575 Figure 12 shows a snapshot of ARRT run for an event of a magnitude of 20 times the 2003  
576 Halloween storm. In this scenario the total BFO dose for event 1 is 1.6 mGy-eq, and it is treated  
577 as an independent event. The onset of event 2 is the same as the original data, as the background  
578 dose rates are elevated with a same factor. As the BFO dose gradually increases to over 100  
579 mGy-eq and then over 250 mGy-eq, the flight note content for “Recommended Crew Actions”,  
580 “Short-term Crew Impacts”, and “Continuing Crew Impacts” change texts according to the  
581 response categories described in Supporting Information, and other contents as well as the table  
582 for the first 48 hours crew impacts are updated at each time step. After events 2-3 initially stops  
583 at 2003-10-31 7:10, the “SPE Status” changes to “Event completed, Crew Monitoring” (yellow  
584 light on). Because the total BFO dose at this stage is 310 mGy-eq, the initial dwelling time is 6.2  
585 days (i.e., 310/50, according to the definition), so the system continues to read on data, do all  
586 kinds of calculation, and update the flight note and ARS response at every time step. If there  
587 were no following events, this monitoring mode would continue till 2003-11-06 12:00, i.e., the  
588 end of the event according to the definition of ARRT.  
589

590 Because event 4 occurred on 2003-11-04 10:25, which is before the end initially determined by  
591 the total dose of events 2-3, the dwelling time set by events 2-3 is redefined according to the  
592 algorithm. When events 4 and 5 kick in, they not only add the total BFO dose, but also nullify  
593 the counter for time points below the dose rate threshold. Because the dwelling time is counted  
594 by the time points below the threshold, it is refreshed during the periods of events 4 and 5. As the  
595 total BFO dose at the end of event 5 is around 337 mGy-eq, the updated dwelling time becomes

596 6.74 days at this stage. That is why the end of the events 2-5 (one episode) goes to 2003-11-12  
597 18:55 (Table 4), far later than the initially determined end time. Such a long time of crew  
598 monitoring phase is quite reasonable as the critical phase of ARS is usually 3-4 weeks after  
599 significant exposure (Hu, 2016). From the plots of ARS severity and blood cell dynamics in  
600 Figure 11, the monitoring phase covers 1/3 of the ARS projection, giving sufficient time for  
601 ground mission control team to estimate possible health effects during the following critical  
602 phase.

603

## 604 **5 Summary and conclusion**

605

606 The health risks of space radiation present the most serious challenges to space exploration, and  
607 the unpredictable ESPEs add significant radiation dose to astronauts in a short period of time,  
608 while rare large events can induce ARS requiring close crew monitoring and management even  
609 during the missions. ARRT was developed to directly use the readings of onboard dosimeters to  
610 project organ doses for the upcoming space explorations, so that any possible ARS risks to the  
611 astronauts can be modelled and monitored in real time, removing dependence on the  
612 measurements by other instruments that may not be able to detect ESPEs along the trajectories of  
613 the spacecrafts. This operational tool represents a good example of effort to transition research to  
614 operation, as many years of works in space radiation measurement and modeling, transport  
615 calculation for high energy particles, and acute radiation responses for human are involved and  
616 elegantly implemented in this compact software to be tested and utilized operationally in the  
617 upcoming Artemis missions.

618

619 To enable ARRT to handle variant scenarios of any possible ESPEs in an automatic manner for  
620 mission operation, two datasets were employed in developing its modules, one involving  
621 historical solar protons recorded over the past four decades and the other using the real-time  
622 telemetric readings of dosimeters onboard ISS. Though vastly different in term of data cadence,  
623 smoothness, and bad data gaps, all events in these datasets can be correctly processed to read and  
624 plot, to project organ doses and ARS risks, and to generate flight notes relevant to the console  
625 operational team. All these tasks are completed with close interactions between multiple modules  
626 developed with many state-of-the-art facilities of full stack web applications. As an ESPE may  
627 last days or even weeks, and all data processing, dose projection, graphic presentation, and text  
628 updates need to be performed in real-time, the computation resource for this tool is very  
629 demanding. Thanks to the fast developing computational techniques such as concurrent data  
630 structures, parallel algorithms, and multi-thread management, as well as product scalability of  
631 cloud computing platforms, which are employed in the developing process, this tool meets the  
632 requirement to project radiation exposure and to provide clinical guidelines in very short time  
633 steps even for the longest event in datasets. All these efforts make this tool eligible to be tested  
634 the upcoming Artemis missions and utilized in future space exploration.

## 635 **Sources of Data and Supplementary Material**

636 Solar proton data:

637 SEPEM: [http://sepem.eu/help/data\\_ref.html](http://sepem.eu/help/data_ref.html)

638 Software:

639 dygraphs: <http://dygraphs.com/>

640

## 641 **Acknowledgements**

642

643 We thank Christopher Mertens and Tony Slaba for the development of the organ dose projection  
644 algorithm for Orion MPCV. The material and shielding thicknesses files of MPCV were  
645 determined by ray tracing the CAD model by Hatem Nounu. Figure 1 was obtained from internal  
646 report by Kerry Lee, and the left panel of Figure 5 was generated by Kathryn Whitman from  
647 SEPEM dataset. This work was supported by KBR Human Health and Performance Contract  
648 (HHPC) NNJ15HK11B.

649

## 650 **References:**

651

652 Feynman, J., T. P. Armstrong, L. Dao-Gibner, and S. M. Silverman (1990), A new interplanetary  
653 proton fluence model, *J. Spacecraft and Rockets*, 27, 403.

654 Fliedner, T. M., I. Friesecke, and K. Beyrer (2001), *Medical Management of Radiation*  
655 *Accidents—Manual on the Acute Radiation Syndrome*. London: British Institute of Radiology.

656 Hu, S., C. Zeitlin, W. Atwell, D. Fry, J.E. Barzilla, and E. Semones (2016), Segmental  
657 interpolating spectra for solar particle events and in situ validation. *Space Weather*, 14 (2016),  
658 pp. 742-753, doi:10.1002/2016SW001476.

659 Fliedner, T.M., D. Graessle, C. Paulsen, K. Reimers (2002), Structure and function of bone  
660 marrow hemopoiesis: mechanisms of response to ionizing radiation exposure. *Cancer Biother.*  
661 *Radiopharm.*, 17, pp. 405-426

662 Hu, S., and F. A. Cucinotta (2011), Characterization of the radiation-damaged precursor cells in  
663 bone marrow based modeling of the peripheral blood granulocytes response. *Health*  
664 *Physics*,101(1), 67–78.

665 Hu, S., and F. A. Cucinotta (2013), Modeling the depressed hematopoietic cells for immune  
666 system under chronic radiation. In L. E. Peterson, F. Masulli and G. Russo (Eds.), *International*  
667 *Meeting on Computational Intelligence Methods for Bioinformatics and Biostatistics* (pp. 26–  
668 36). Berlin, Heidelberg: Springer.

669 Hu, S., J. E. Barzilla, and E. Semones (2020), Acute radiation risk assessment and mitigation  
670 strategies in near future exploration space flights, *Life Sciences in Space Research*, 24, 25-33

671 Hu, S., M.-H. Y. Kim, G. E. McClellan, and F. A. Cucinotta (2009), Modeling the acute health  
672 effects of astronauts from exposure to large solar particle events. *Health Physics*,96(4), 1–12.

673 Hu, S., O. A. Smirnova, and F. A. Cucinotta (2012), A biomathematical model of lymphopoiesis  
674 following severe radiation accidents—Potential use for dose assessment. *Health Physics*,102(4),  
675 425–436.

676 Hu, S., W. F. Blakely, and F. A Cucinotta (2015), HEMODOSE: A biodosimetry tool based on  
677 multi-type blood cell counts. *Health Physics*,109(1),54–68.

678 Hu, S. (2016), Linking doses with clinical scores of hematopoietic acute radiation syndrome.  
679 *Health Physics*,111(4), 337–347.

680 Jiggins, P. T. A., S. B. Gabriel, D. Heynderickx, N. B. Crosby, A. Glover, and A. Hilgers  
681 (2012), ESA SEPEM project: Peak flux and fluence model, *IEEE Trans. Nucl. Sci.*,59,4

682 Kim, M.H., S. Hu, H. N. Nounu, and F. A. Cucinotta (2010), Development of Graphical User  
683 Interface for ARRBOD (Acute Radiation Risk and BRYNTRN Organ Dose Projection).

684 Hanover, MD: Center for Aerospace Information; NASA TP -2010-216116.

685 Kroupa, M., A., Bahadori, T., Campbell-Ricketts, A. Empl, S. M., Hoang, J., Idarraga-Munoz, et  
686 al. (2015). A semiconductor radiation imaging detector for space radiation dosimetry. *Life*  
687 *Sciences in Space Research*,6, 69–78.

688 Matheson, L. N., M. A. Dore, G. H. Anno, and G. E. McClellan (1998). Radiation-induced  
689 performance decrement (RIPD): User’s manual, version 2.0 (DNA-TR-95-91). Alexandria, VA:  
690 Defense Nuclear Agency.

691 Mertens, C. J., B. T. Kress, M. Wiltberger, S. R. Blattnig, T. S. Slaba, S. C. Solomon, and M.  
692 Engel (2010), Geomagnetic influence on aircraft radiation exposure during a solar energetic  
693 particle event in October 2003, *Space Weather*, 8, S03006, doi:10.1029/2009SW000487.

694 Mertens, C. J., T. C. Slaba, and S. Hu (2018), Active dosimeter-based estimate of astronaut acute  
695 radiation risk for real-time solar energetic particle events. *Space Weather* 16, 1291–  
696 1316. <https://doi.org/10.1029/2018SW001971>

697 NASA (2014), Space Flight Hum. Syst. Stand. 1. Revision A: Crew Health. NASA Technical  
698 Standard NASASTD-3001, National Aeronautics and Space Administration, Washington, DC

699 NAS/NRC (1970), Radiation Protection Guides and Constraints for Space-Mission and Vehicle-  
700 Design Studies Involving Nuclear Systems. National Academy Press, Washington, DC

701 NOAA (2020), Solar Proton Events Affecting the Earth Environment,  
702 <https://umbra.nascom.nasa.gov/SEP/>, Space Weather Predict. Cent., Boulder, Colo., accessed on  
703 2020-03-17

704 NRC (1967), Radiobiological factors in Manned Space flight, Report of Space Radiation Study  
705 Panel of the Life Sciences Committee, Langham WH (ed), National Academy Press,  
706 Washington, DC

707 Raukunen, O., R. Vainio, A. J. Tylka, W. F. Dietrich, P. Jiggins, D. Heynderickx, et al. (2018),  
708 Two solar proton fluence models based onground level enhancement observations.*Journal of*  
709 *Space Weather and Space Climate*, 8, A04.

710 Robinson, Z. D., J. H. Adams, M. A. Xapsos, and C. A. Stauffer (2018), Database of episode-  
711 integrated solar energetic proton fluences. *J. Space Weather Space Clim.*, 8 A24. DOI:  
712 <https://doi.org/10.1051/swsc/2018013>

713 Slaba, T. C., J. W. Wilson, F. F. Badavi, B. D. Reddell, and A. A. Bahadori (2016), Solar proton  
714 exposure of an ICRU sphere within a complex structure: Ray-trace geometry. *Life Sciences in*  
715 *Space Research* 9, 77–83.

716 Townsend, L. W., J. H. Adams, S. R. Blattnig, D. J. Fry, I. Jun, M. S. Cloudsley, et al. (2018),  
717 Solar particle event storm shelter requirements for missions beyond low Earth orbit. *Life*  
718 *Sciences in Space Research*,17, 32–39.

719 Townsend, L.W., J. L. Shinn, and J. W. Wilson (1991), Interplanetary crew exposure estimates  
720 for the August 1972 and October 1989 solar particle events. *Radiat. Res.* 126, 108-110.

721 Tylka, A. J., J. H. Adams, P. R. Boberg, B. Brownstein, W. F. Dietrich, E. O. Flueckiger, E. L.  
722 Petersen, M. A. Shea, D. F. Smart, and E. C. Smith (1997), CREME96: A revision of the cosmic  
723 ray effects on micro-electronics code, *IEEE Trans. Nucl. Sci.*,44, 2150–2160.

724 Wilson, J. W., T. C. Slaba, F.F. Badavi, B.D. Reddell, and A.A. Bahadori (2016), Solar proton  
725 exposure of an ICRU sphere within a complex structure: Combinatorial geometry. *Life Sciences*  
726 *in Space Research* 9, 69–76.

727